The suitability of silicon carbide for photocatalytic water oxidation

M. Aslam, M. T. Qamar, Ikram Ahmed, Ateeq Ur Rehman, Shahid Ali, I. M. I. Ismail & Abdul Hameed

Applied Nanoscience

ISSN 2190-5509

Appl Nanosci
DOI 10.1007/s13204-018-0772-2

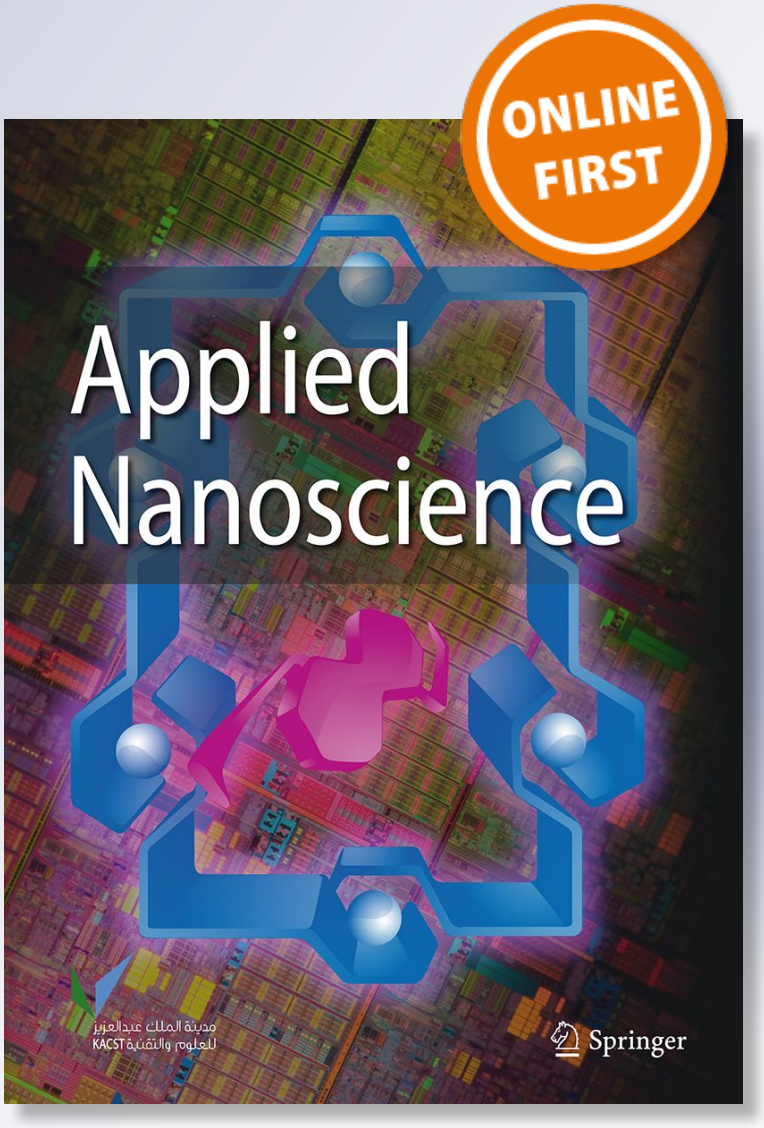

Springer

Applied Nanoscience
https://doi.org/10.1007/s13204-018-0772-2

ORIGINAL ARTICLE

The suitability of silicon carbide for photocatalytic water oxidation

M. Aslam[1] · M. T. Qamar[2] · Ikram Ahmed[3] · Ateeq Ur Rehman[4] · Shahid Ali[5] · I. M. I. Ismail[1,6] · Abdul Hameed[1,7]

Received: 8 January 2018 / Accepted: 12 April 2018

Abstract

Silicon carbide (SiC), owing to its extraordinary chemical stability and refractory properties, is widely used in the manufacturing industry. Despite the semiconducting nature and morphology-tuned band gap, its efficacy as photocatalysts has not been thoroughly investigated. The current study reports the synthesis, characterization and the evaluation of the capability of silicon carbide for hydrogen generation from water splitting. The optical characterization of the as-synthesized powder exposed the formation of multi-wavelength absorbing entities in synthetic process. The structural analysis by XRD and the fine microstructure analysis by HRTEM revealed the cubic 3C-SiC (β-SiC) and hexagonal α-polymorphs (2H-SiC and 6H-SiC) as major and minor phases, respectively. The Mott–Schottky analysis verified the n-type nature of the material with the flat band potential of − 0.7 V. In the electrochemical evaluation, the sharp increase in the peak currents in various potential ranges, under illumination, revealed the plausible potential of the material for the oxidation of water and generation of hydrogen. The generation of hydrogen and oxygen, as a consequence of water splitting in the actual photocatalytic experiments, was observed and measured. A significant increase in the yield of hydrogen was noticed in the presence of methanol as h^+ scavenger, whereas a retarding effect was offered by the Fe^{3+} entities that served as e^- scavengers. The combined effect of both methanol and Fe^{3+} ions in the photocatalytic process was also investigated. Besides hydrogen gas, the other evolved gasses such as methane and carbon monoxide were also measured to estimate the mechanism of the process.

Keywords Silicon carbide · Water splitting · Hydrogen generation · h^+–e^- scavenger

Introduction

The demand for environment friendly, clean and renewable energy sources has gained substantial attention with the declining environmental health of the sphere due to the consumption of fossil fuel reserves. Although hydrogen is the most idyllic energy carrier in this regard without releasing any toxic offshoots to solve the global energy issue (Chen et al. 2010; Muradova and Veziroglub 2008), however, currently, the majority of the hydrogen production is mainly extracted from the non-renewable fossil fuels with the addition of carbon dioxide to the environment (Balat and Kırtay 2010; Kothari et al. 2008). Now, the efforts are underway to replace the fossil fuels with the environmental-friendly ingredients for the generation of hydrogen (Çelik and Yıldız 2017; Shankar and Shikha 2017). In the recent years, the splitting of water into hydrogen and oxygen by photocatalysis via powdered photocatalytic water splitting has attracted incredible consideration to conquer clean and carbon-free hydrogen fuel (Frei 2017; Hisatomi and Domen 2017; Chen et al. 2017). The photocatalytic mechanism

✉ Abdul Hameed
ahfmuhammad@gmail.com; afmuhammad@kau.edu.sa

1 Centre of Excellence in Environmental Studies (CEES), King Abdulaziz University, Jeddah 21589, Saudi Arabia

2 Department of Chemistry, Forman Christian College (A Chartered University), Ferozepur Road, Lahore 54600, Pakistan

3 Department of Applied Chemistry, Government College University, Faisalabad 38000, Pakistan

4 School of Chemical Engineering, The University of Queensland, Saint Lucia, QLD 4067, Australia

5 Centre of Excellence in Nanotechnology (CENT), King Fahd University of Petroleum and Minerals, Dhahran 31261, Saudi Arabia

6 Chemistry Department, Faculty of Science, King Abdulaziz University, Jeddah 21589, Saudi Arabia

7 National Centre for Physics, Quaid-e-Azam University, Islamabad 44000, Pakistan

Published online: 18 April 2018

using semiconductor photocatalyst is based on the absorption of the incident photons with the simultaneous generation of reactive sites on the surface of the semiconductor is regarded as a potential tool to overcome the energy barrier that hinders the stripping of hydrogen from water, however, austerely reliant on the energy gap and the associated electrochemical potentials (Moon et al. 2000; Fujishima and Honda 1971). Various classes of semiconductor materials in the form of oxides (such as d^0, d^{10}, and f^0 metal oxide photocatalyst) and non-oxides (such as metal sulfides, nitrides, oxysulfides and oxynitrides) photocatalysts have been used for photocatalytic hydrogen generation (Ahmad et al. 2015; Chen et al. 2010; Chen et al. 2010). However, still, the scientific community has either concentrated on the alteration of existing photocatalysts to develop highly stable, ecofriendly, and economically viable photocatalysts or the exploration of new photocatalytic materials for enhanced hydrogen evolution. Consequently, along with other potential contenders, silicon carbide (SiC), despite having semiconducting nature, high chemical stability, environment-friendly- (Wang et al. 2014a, b), morphology-tuned-band gap and suitable band edge positions, has not been thoroughly investigated for its photocatalytic water-splitting efficacy. Silicon carbide, an important non-oxide ceramic and promising metal-free photocatalyst, has a wide range of its industrial applications in various fields due to its unique properties such as suitable band gap (2.3–3.3 eV), high melting point (2827 °C), outstanding chemical oxidation resistance, surface area, mechanical strength and high thermal stability (Shi et al. 2006; Ravi et al. 2000; Pierre 2002; Madar 2004; Zhu et al. 2001; Nakamura et al. 2004; Mikolaj and Pawel 2001; Ishikawa et al. 1998; Yoshida et al. 1998; Fu et al. 2005). Although the polymorphs of SiC have been a substrate of interest as anode material in the photoelectrocatalytic generation of hydrogen with the promising performance (Walter et al. 2010; van Dorp et al. 2009; Zhu et al. 2009), however, the studies on the evaluation of SiC solely are limited rather than combination with other co-catalyst, as the water splitting photocatalyst (Shcherban 2017; Xie et al. 2018). Various catalysts have been used to make a composite with SiC for the application in photocatalytic water splitting. Recently, Dang et al. reported the enhanced photocatalytic and photoelectrochemical water splitting over one-dimensional Au/SiC heterojunction nanocomposite (Dang et al. 2018). Jiang et al. prepared nickel/SiC nanowire composite for the efficient hydrogen production through photoelectrocatalytic water-splitting process (Jiang et al. 2017). Pt and IrO_2 co-catalyst on the surface of SiC was synthesized by Wang et al. for the improved hydrogen evolution in the presence of sacrifice reagents (Wang et al. 2017a, b). Similarly, g-C_3N_4/SiC (Chang et al. 2018; Wang et al. 2017a, b, 2013), Ag_3PO_4/Ag/SiC (Chen et al. 2015), Pt/SiC (Wang et al. 2014a, b), Sic/CdS (Peng et al. 2014), Co_3O_4/SiC (Lee et al. 2018) etc. photocatalyst were also been studied by the researchers in the application of photocatalytic water splitting. With the suitability of the band potentials and the morphology-tweaked band gap, SiC photocatalyst also has the pronounced capability to split water under illumination (Saraswat et al. 2018; Zhang et al. 2014; Hao et al. 2013; Liu et al. 2012; Yasuda et al. 2012; van Dorp et al. 2009). The conduction band edge of SiC also makes it even superior to TiO_2 and CdS for the generation of hydrogen (Saraswat et al. 2018; Hatakeyama and Kanzaki 1990).

The current study comprised of the synthesis, characterization, and the detailed evaluation of the photocatalytic activity of as-synthesized SiC for the generation of hydrogen from water splitting. The SiC powder was optically characterized by UV–visible diffuse reflectance (DR), photoluminescence (PL) and Raman spectroscopy. The phase purity, structural parameters and fine microstructure analysis of the material was performed by X-ray diffraction (XRD) and high-resolution transmission electron microscopy (HRTEM), whereas field emission electron microscopy (FESEM) was employed for textural and morphological examination. The chemical environment of each component of SiC and the formation of additional entities during the synthetic route was estimated by X-ray photoelectron spectroscopy (XPS). The charge transport in the material under illumination and the band edge positions of the valence and conduction bands were assessed by electrochemical impedance spectroscopy (EIS) and Mott–Schottky analysis, respectively. The suitability of the material for water oxidation and hydrogen reduction was initially estimated by electrochemical tools and finally subjected to actual photocatalytic water-splitting experiments. The evolved gases were measured and quantified by gas chromatography. The effect of the eminent photogenerated e^- and h^+ scavenging species such as methanol and Fe^{3+} ions, on gas evolution, was also assessed. The experimental evidences were amassed to explain various processes occurring under illumination at the surface of the catalyst and in the bulk.

Experimental details

The procedure that we adopted is similar to one reported in the literature (Raman et al. 1995; Najafi et al. 2012; Li et al. 2000), however, modified with the addition of surfactant for better control of the particle size. In a typical synthesis, the stoichiometric amount of phenolic resin was dissolved in 100 ml ethanol followed by the addition of triton X-100 as a surfactant under the constant stirring for 1 h at 50 °C. The solution containing 100 ml of tetraethyl orthosilicate (Sigma-Aldrich), ethanol and water was slowly added into the phenolic resin solution. The solution was stirred for 2 h to attain the homogeneity. The mixture was refluxed

at 100 °C to ensure the formation of $Si(OH)_4$ with removal of volatile solvent and alcohols. The solution containing $Si(OH)_4$ and resin was refluxed for a prolonged time of 180 min. The resultant wet-gel was aged and dried at 100 °C in an oven. Finally, to remove the structural impurities, the powder was pyrolyzed at 1600 °C in a tubular furnace for 6 h with a heating rate of 10 °C/min under an argon atmosphere of 75 ml/min to obtain the gray color SiC powder.

The optical investigations of the as-synthesized SiC that included the acquiring of solid-state absorption and the diffuse reflectance spectra, was performed by a Perkin Elmer Lambda 650, UV–visible diffuse reflectance spectrophotometer (DRS) in the wavelength range of 190–900 nm. The *%R* data from the DRS spectra were subjected to Kubelka–Munk transformation for the evaluation of the band gap of the material. The excitation–de-excitation behavior of the material was evaluated by fluorescence spectro-fluorophotometer, FS-2, Sinco, Korea, at an excitation wavelength of 250 nm, whereas the Raman pattern was assimilated by a DXR Raman Microscope, Thermo Scientific, USA, equipped with 532 nm laser as the excitation source at 6 mW power. For the structural analysis, the powder XRD pattern of synthesized powder was by Xpert X-ray powder diffractometer (Philips PW1398) with Cu $K\alpha$ radiation source from 10° to 90° (2θ) with a step of 0.05°. The crystallite size was evaluated by applying Scherer's equation on the most intense reflection. The variations in the chemical environment of Si and C in synthesized were estimated by X-ray photoelectron spectrometer (PHI 5000 VersaProbe II, ULVAC-PHI Inc.) in the binding energy range of 0–1100 eV. The morphology of the synthesized powder was reviewed by field emission scanning electron microscope (FEI, Quanta FEG 450, Quorum Q150R ES, Quorum technologies, whereas the fine microstructure analysis was performed by high-resolution transmission electron microscope (JEM-2100 JEOL, USA) at different resolutions.

The charge transport in the synthesized material both in the dark and under illumination was evaluated by electrochemical impedance spectroscopy (EIS), whereas the Mott–Schottky analysis was performed to evaluate the flat band potential and to specify the semiconducting nature. The water oxidation and hydrogen production ability of the synthesized material was investigated by cyclic voltammetric analysis in positive and negative potential range. For electrochemical measurements, a VSP multi-channel potentiostat (Bio-logic Science Instrument, USA) equipped with glassy carbon (GC), platinum and Ag/AgCl saturated electrodes as working, counter and reference electrodes, respectively. For the modification of GCE (working electrode), a sonicated dispersion of catalyst in chloroform was coated at the surface. The electrochemical impedance spectroscopy (EIS) of the SiC was performed in the frequency range of 100 mHz to 100 kHz with an amplitude of 10 mV at a bias of + 0.23 V vs. Ag/AgCl. The fitting of EIS Nyquist plots was achieved by Zfit (Ec-lab software, Bio-logic Science Instruments, USA). Except for CV analysis which was performed in the basic medium for water oxidation and hydrogen reduction in the neutral medium, all the other measurements were executed in 0.1 M KCl solution. A 50-W halogen lamp was used as a source for the measurements under illumination.

The photocatalytic water-splitting ability of as-synthesized SiC was studied in a 1000 cm^3 Pyrex® glass reactor equipped with inlets and outlets for gasses, magnetic stirrer, and water-cooled quartz immersion tube. A 700-W variable power medium pressure mercury lamp (12% UV), operated at 300 Ws, was used as illumination source. The evolved gases were measured by gas chromatography (GC) coupled with the glass reactor equipped with molecular sieve 5A plot column and thermal conductivity detector (TCD). Argon gas was used as a carrier as well as purging gas. In a typical water-splitting experiment, a 300 mg/L of the SiC catalyst was suspended in the reactor and purged with Ar gas for the complete removal of air. The amount of the catalyst was optimized on the basis of the 5–7% transmitted light escaping the reactor at the lamp power of 300 W. The purging gas was analyzed at the regular intervals and the exposure of the catalyst initiated with the complete depletion of oxygen and nitrogen. The gas samples from the reactor were analyzed after regular intervals to measure the evolved gasses by GC. To study the effect of methanol as "hole scavengers" on hydrogen production, the experiment was performed in 1% methanol solution, whereas the effect of electron scavengers (Fe^{3+} ions) was estimated by adding 50 ppm of metal ion solution.

Results and discussion

As mentioned earlier, although the synthetic route was adopted from the literature, it was, however, modified for ease and user-friendly approach. The Triton X-100 was used as a surfactant to control the morphology of the synthesized gray powder. The characterization of the as-synthesized powder by various analytical tools is discussed below.

Being the preliminary requirement for the photocatalytic applications, the absorption spectra of the as-synthesized powder was recorded by diffuse reflectance spectroscopy and presented in Fig. 1a. The absorption pattern revealed the dual absorption onsets corresponding to multiple electronic states indicating the existence of more than one polytypes of SiC in the sample. The dominant absorption edge was witnessed in the 400–500 nm range, whereas the minor onset appeared in 300–400 nm region that depicted the wide photon absorption range of the material, therefore, the multiple entities with the discrete band arrangements were presumed. The valence band in SiC is formed by the C2p

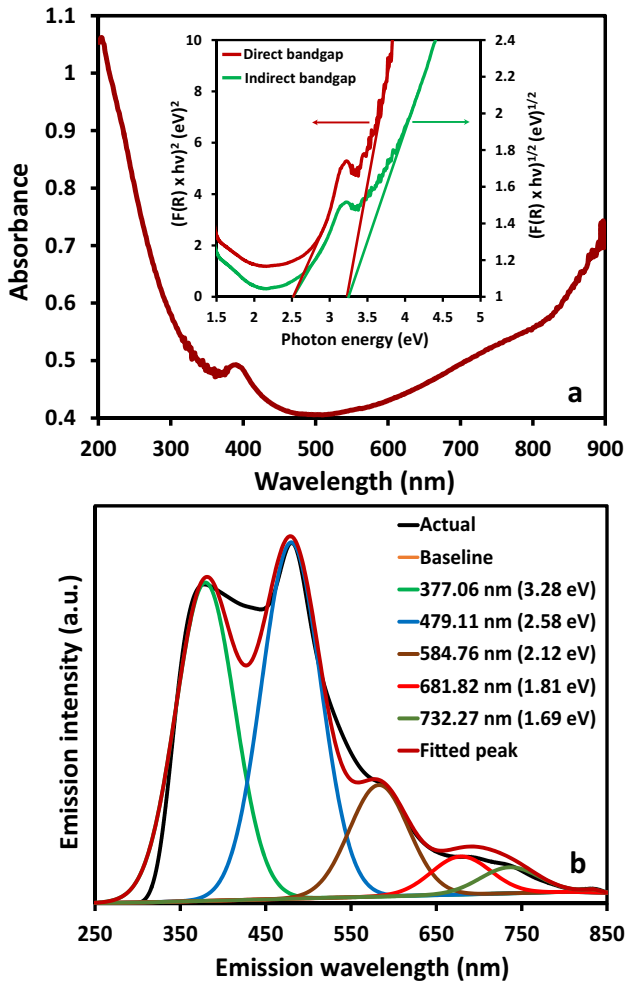

Fig. 1 **a** The solid-state absorption spectra of as-synthesized SiC. The inset shows the graphical evaluation of the direct and indirect band gap **b** the fitted PL spectra of the SiC powder showing the probable de-excitations

orbitals (HOMO), whereas the Si3p might be designated as conduction band (LOMO). The variations in the spacing (band gap energy) are reported as the function of the atomic arrangement in the crystal structure (Fan and Chu 2014). The band gap energies of both the prevalent polytypes identified in the absorption spectra were graphically evaluated by applying a Kubelka–Munk transformation [$F(R)$] to the $\%R$ data extracted from the experimental diffuse reflectance spectra. The plots of $[F(R)\times h\nu]^n$ versus $h\nu$ (photon energy) ($n=0.5$ for indirect and $n=2$ for direct electronic transitions) are presented in the inset of Fig. 1a. The extrapolation of the straight portion of the onsets resulted in the band gap energies of photon absorbing entities in the sample. The evaluated direct band gaps of ~ 2.5 and ~ 3.25 eV were in close agreement to that reported in the literature for the cubic and hexagonal polytypes of SiC (Wenzien et al. 1995; Persson and Lindefelt 1997). The close synergy between the direct and indirect band gap energies rules out the possible existence of the intraband states in the sample thus leading to defined band structure.

The band structure and the possible existence of more than one polytypes in the synthesized SiC were further investigated by PL spectroscopy by exciting the sample at 250 nm. As presented in Fig. 1b, the acquired diffused PL spectra in the emission range of 250–850 nm was deconvoluted and fitted to expose the probably hidden transitions. The deconvolution revealed the peaks at the ~ 377.06, ~ 479.11, ~ 584.76, ~ 681.82 and ~ 732.27 nm corresponding to the energies of ~ 3.28, ~ 2.58, ~ 2.12, ~ 1.81 and ~ 1.69 eV. Being corresponding to the band gap de-excitation, the peaks that appeared in the 300–500 nm were of particular interest. The close agreement of the associated energies of ~ 3.28 and ~ 2.58 eV with those evaluated by the diffused reflectance spectroscopy not only validated the suitability of the adopted technique but also authenticated the existence of more than one polytype in the sample. The peaks in the low energy region were assigned to the de-excitation of the electron trapped in the carbon-associated defects on their way back to the valence band.

As Raman spectroscopy can be used to identify the polytypes in the sample (Freitas JA Jr 1995), as shown in Fig. 2a, the as-synthesized SiC was subjected to Raman analysis in the wide-scanning range of 100–2900 cm^{-1}. Besides several minor peaks, the major peaks appeared at 792.37, 915.79, 1354.54, 1595.57 and 2678.41 cm^{-1}. As the origin of the appeared Raman modes is well discussed in the literature (Freitas and Moore 1998), therefore, the significance with respect to the evaluation of the phase purity will be discussed. The peaks at 792.37 and 915.79 cm^{-1} represent the TO and LO bands of cubic SiC, whereas the bands at 1354.54 and 1595.57 cm^{-1} characterize the D and G material of the same. The observed values with minor variations were in close agreement with the literature values (Qi et al. 2014). The peak at 2678.41 cm^{-1} was assigned to hexagonal SiC as the appearance of the same is also supported by the literature (Huang et al. 2010; Lin et al. 2012). Additionally, the growth of the peak is also associated with the successive addition of layers. The cluster of low-intensity peaks in 300–600 cm^{-1} regions was also assigned to the hexagonal SiC.

The XRD pattern acquired to identify the polytypes present in the as-synthesized SiC is presented in Fig. 2b. The major reflections at 2θ values of ~ 35.55°, ~ 41.51°, ~ 59.95°, ~ 71.76°, ~ 75.32° were attributed to the (1 1 1), (2 0 0), (2 2 0), (3 1 1) and (2 2 2) faces and matched with cubic 3C SiC (JCPDS# 73-1665). The careful identification of the minor reflections at 2θ values of ~ 33.75°, ~ 41.45° and ~ 67.41° indicated the minor presence of α phase and matched with 6H SiC with hexagonal geometry (JCPDS# 75-1541). The observed reflections both for 3C and 6H SiC were in close

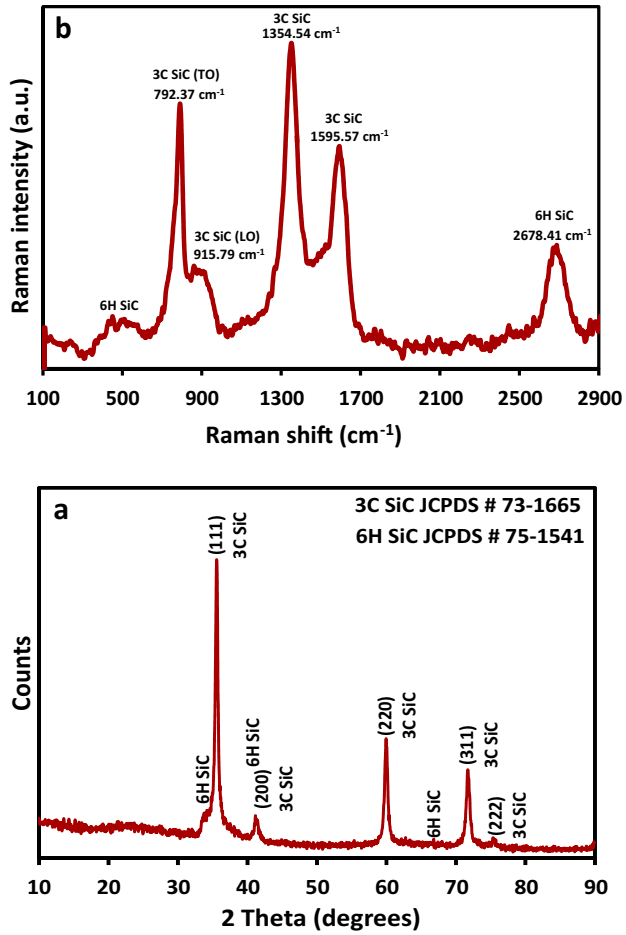

Fig. 2 **a** The Raman spectra and **b** XRD pattern of the as-synthesized SiC

agreement with those reported in the literature (Iwanowski et al. 1999). A crystallite size of 24.2 nm was evaluated using the parameters of the most intense reflection at ~ 35.55°. The absence of reflections ensures the complete consumption of elemental Si in SiC formation. The XRD analysis endorsed the formation of dual phase SiC with 3C SiC (β-SiC) as the major phase and 6H SiC (α-SiC) as a minor phase. Besides the polytypes mentioned above the extremely low-intensity reflections due to 2H and 4H SiC were also noticed.

The FESEM images of the synthesized SiC at various magnifications are compared in Fig. 3. At low magnification, the particles appeared as the porous spheres (Fig. 3a–c) that exposed as the aggregates of smaller particles at higher magnifications. Due to the surface charging the further magnification resulted in the blurred images with no significant information, therefore, the morphology and microstructure analysis of the as-synthesized SiC was carried out by transmission electron microscopy (TEM). The high-magnification TEM images exposing the acceptable morphology are presented in Fig. 4a, b, where the particles of various sizes having the similar shape are observable. The average particle size of the particles ranges from 10 to 40 nm. Interestingly, the shapes of the particles were the combination of the cubic and hexagonal geometry. The HRTEM images (Fig. 4c) also corroborated the above-mentioned findings, where the atomic scale focusing of the single crystal revealed the discrete dual fringes. These configurations representing 3C SiC and 6H SiC are marked by green and red arrows on Fig. 4c. The SAED pattern of the as-synthesized SiC is presented in Fig. 4d, where the additional low-intensity reflections other than 3C SiC supported the findings of XRD and consequently verified the co-existence of the polytypes belonging to the hexagonal α phase.

The comparison of the wide angle XPS survey scans of the as-synthesized SiC in the binding energy range of 0–1200 eV, before and after argon etching, is presented in Fig. 5, where the peaks corresponding to the respective components of SiC are evident. As the material was processed in the air for calcination, the appearance of O1 s peak exposed the oxidation of the surface entities. Apparently, no significant shift in the comparison of the individual survey scans before and after etching was witnessed. However, as presented in the inset of Fig. 5, the comparison of the high-precision scans revealed a blue shift of the magnitude of 0.4–0.6 eV in the binding energies of Si2p and C1 s core levels was observed, whereas the binding energy of O1 s core level remains unchanged. The enhanced purity level of the sample after the removal of the surface layer consisting of the oxygenated entities is the probable reason of the effect (Wanga et al. 2012). The decreased intensity of O1 s peak after etching also supported the same finding. Additionally, the asymmetry in the core level peaks indicated the entrapment of the additional peak origination from the chemically different environment. The deconvolution and the fitting of C1 s core levels before and after the etching, as presented in Fig. 6a, b, revealed the major peak corresponding to Si–C bond at the binding energy of ~ 283.97 eV, whereas the expected low-intensity peaks at the binding energy values of ~ 285.03 and ~ 285.82 eV were assigned to C–C and C–O bonds, respectively. A mild increase in the intensity of Si–C, whereas a corresponding decrease was noticed for C–C and C–O peak after etching. The observed values were in close agreement with the literature values (Xue et al. 2008). The high-resolution fitted Si2p core level peaks for the as-synthesized SiC, before and after the etching, are presented in Fig. 6c, d. The deconvolution revealed the peaks at ~ 100.71 and ~ 102.61 eV was assigned to Si–C and Si–O bonds in SiC. A mild decrease in the intensity of the Si–O peak was witnessed after etching. An intense, broad and asymmetric O1 s peak at the binding energy of ~ 532.07 eV (Fig. 6e) representing O–Si–C bonds was evidenced for the sample before etching. The fitting revealed

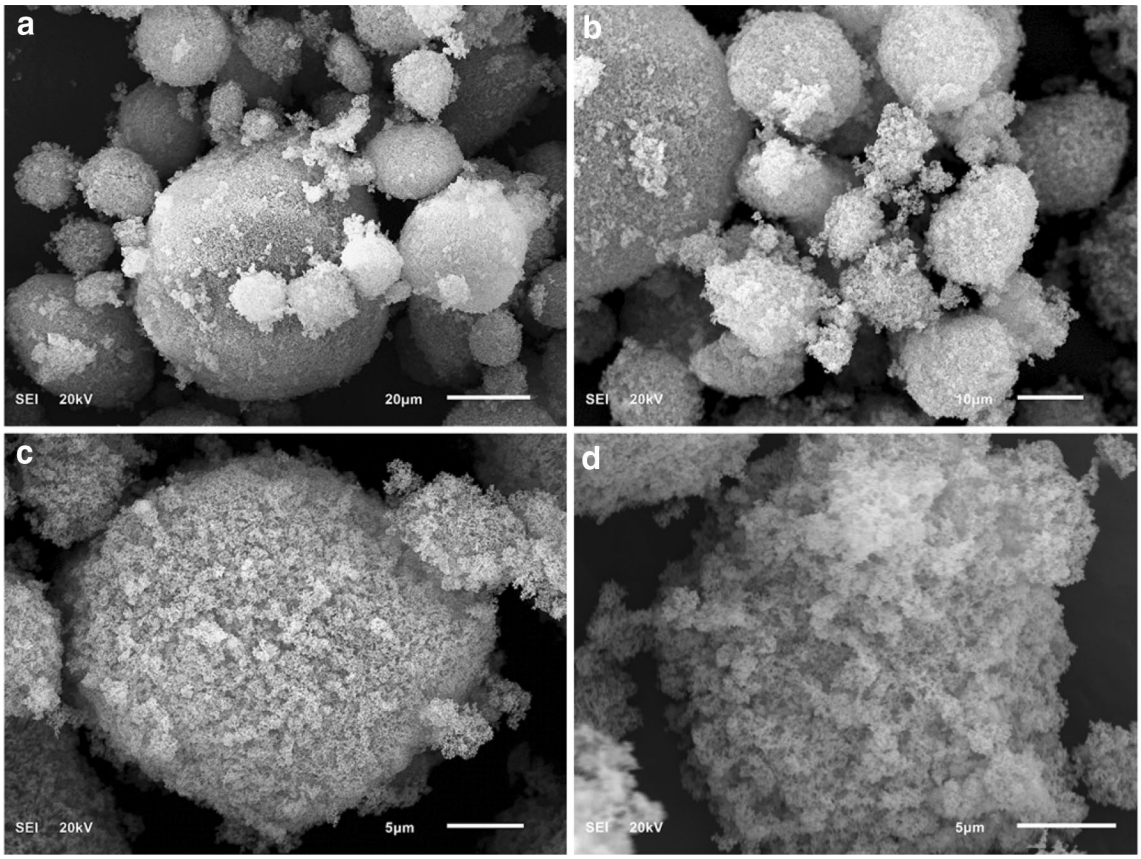

Fig. 3 The comparison of the FESEM images of as-synthesized SiC at various magnification

the additional peaks at the binding energies of ~ 531.21 and ~ 533.11 eV, which were assigned to O–C and O–Si bond in the material. A decrease intensity of the peaks was witnessed after the etching.

In the photocatalytic process, the ease of transport and transfer of photogenerated charge carriers, especially electrons, determine the intrinsic efficiency of the photocatalyst. Among the electrochemical tools, electrochemical impedance spectroscopy (EIS) is regarded as the power technique for the estimation of the resistance offered by the material to the photogenerated charge carriers. The comparison of the Nyquist plots of the fitted EIS spectra of the as-synthesized SiC, in the dark and under illumination, is presented in the Fig. 7a, whereas Randal's circuit used for the fitting is presented in the inset of the same. A substantial decrease in the diameter of the semicircle under illumination as compared to that in the dark depicted the ease of transport to the photon-generated electron to the surface of the electrode. The observation depicted the suitability of the material for a better charge transport and ease of electron transfer. In aqueous phase, photocatalytic processes besides the ease of charge transport, the suitability of the potential associated with the band edges for water oxidation and reduction of adsorbed entities is equally important. The band edges of the synthesized SiC were evaluated by applying the Mott–Schottky analysis to the staircase potential electrochemical impedance spectroscopy (SPIES). The graphical evaluation of the flat band potential (V_{fb}) from the Mott–Schottky plot is presented in Fig. 7b. Interestingly, the presence of the onset of the potential in the negative potential region disclosed the n-type nature of the synthesized material. A similar finding regarding the n-type semiconducting nature of SiC has already been reported in the literature (Sachsenhauser et al. 2016). As the flat band potential (V_{fb}) of the n-type semiconductors directly corresponds to the potential of the conduction band edge (Qamar et al. 2017), the value − 0.7 V was assigned to the conduction edge of the synthesized powder. Consequently, the potential of valence band edge emerged at + 1.8 V. The close agreement with the minor variations, probably due to the dissimilar experimental procedure, validated the authenticity of the adopted experimental procedure (Lauermann et al. 1997). The synthesized material was subjected to cyclic voltammetry for the estimation of the water oxidation and hydrogen reduction ability, in the dark and under illumination, before being subjected to actual photocatalytic water-splitting experiments. The current–potential

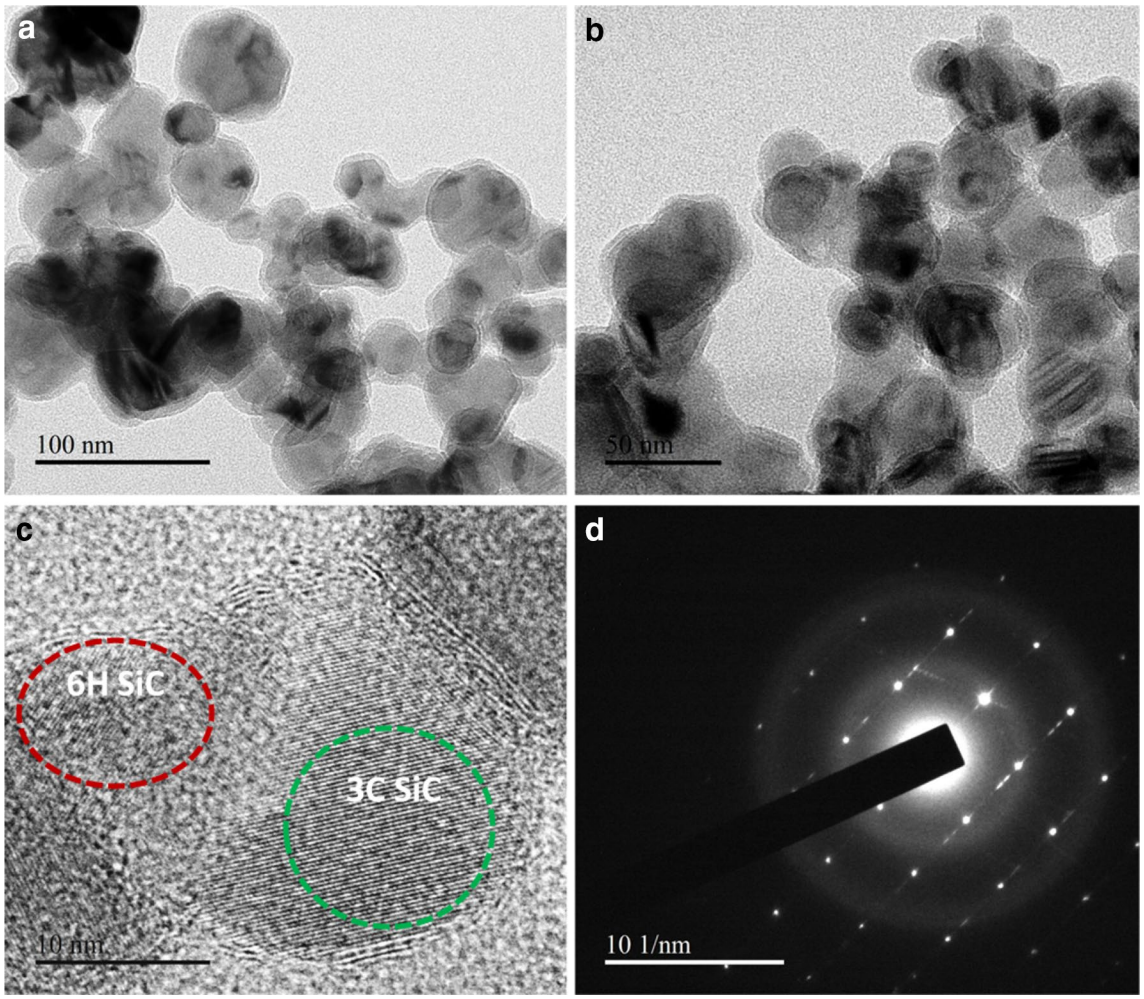

Fig. 4 **a**, **b** The typical TEM images, **c** the HRTEM images targeting the single crystal and **d** the SAED pattern of as-synthesized SiC. The atomic patterns for 3C SiC and 6H SiC in the sample are identified green and red circles, respectively, on **c**

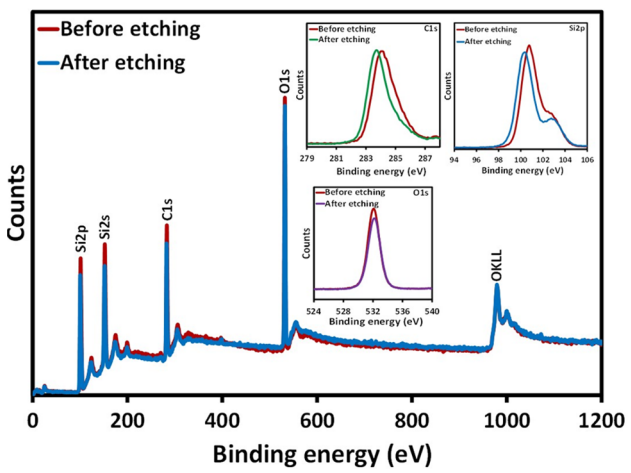

Fig. 5 The comparison of the XPS survey scans of SiC powder before and after etching. The inset shows the variation in the binding energies of C1 s, Si2p, and O1 s core levels

(*I*–*V*) in the dark and under illumination are compared in Fig. 7c. The sharp increase in the peak current with the shifting of the inset potential towards the positive potential region, under illumination, as compared to that of dark elaborated the strong water-oxidizing capacity of the material. As presented in Fig. 7d, the significant increase in the current in the negative potential area supported the acceptable ability to produce hydrogen. In conclusion, the ease of electron transport, suitable band edges, the water oxidation potential and hydrogen-producing ability predicted the suitability of the synthesized material for the photocatalytic splitting of water.

The photocatalytic splitting of water into its components, i.e., O_2 and H_2 is based on the oxidation of adsorbed water molecules by the photogenerated holes (h^+) and the reduction of the in situ-generated H^+ ions by the conduction band electrons at the surface of the photocatalyst to generate hydrogen radicals (Maeda and Domen 2010; Kudo and

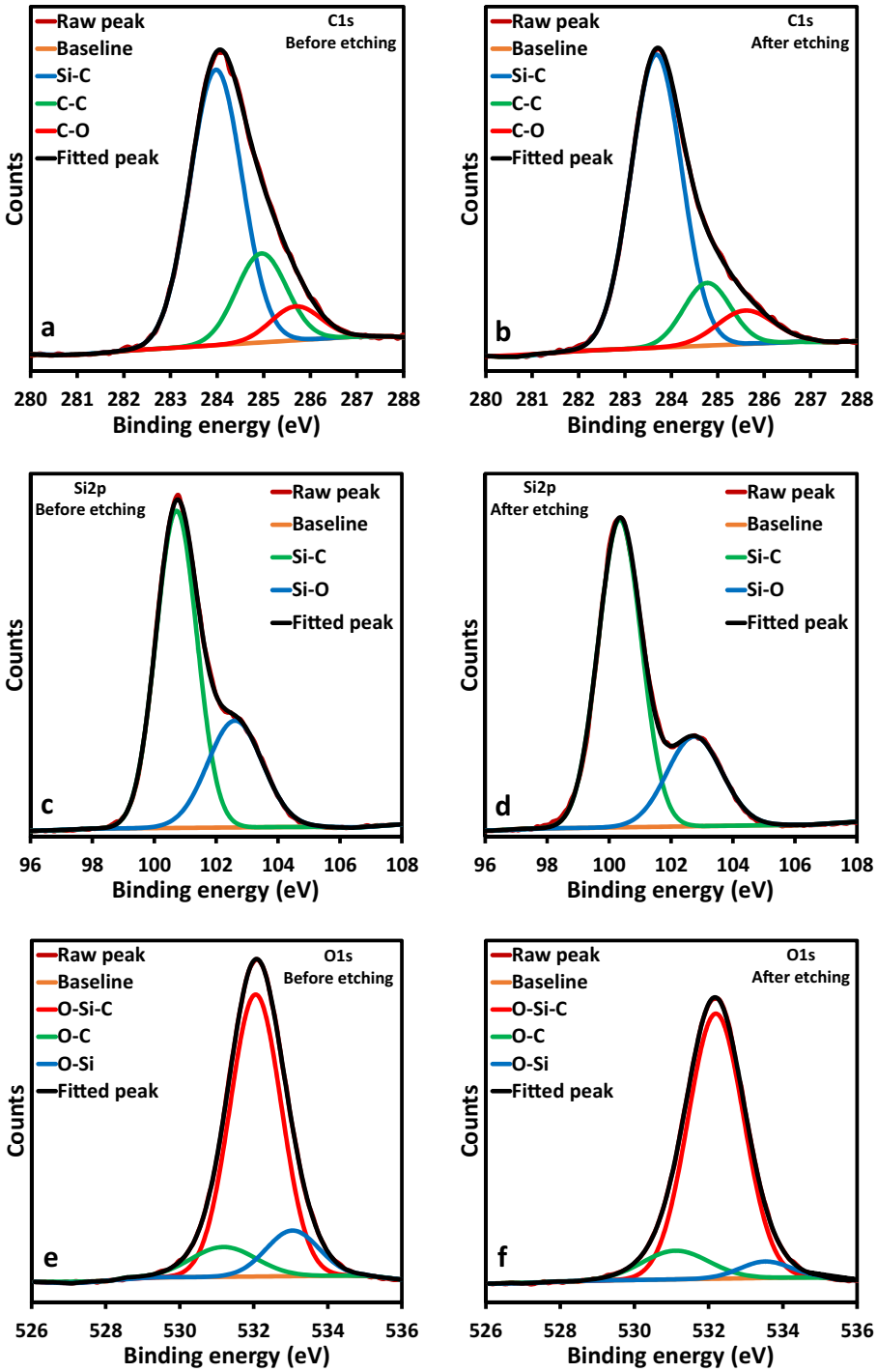

Fig. 6 The comparison of the deconvoluted fitted spectra of C1 s, Si2p and O1 s core levels after depth profiling

Miseki 2009; Ni et al. 2007). The same may be represented by the set of Eqs. (1–3) given below.

$$SC \xrightarrow{h\upsilon > E_g} SC(h^+_{vb} + e^-_{cb}), \quad (1)$$

$$H_2O + h^+_{vb} \rightarrow H_2O^+ \rightarrow OH^{\cdot} + H^+, \quad (2)$$

$$H^+ + e^-_{cb} \rightarrow H^{\cdot}. \quad (3)$$

In the bulk, the combination of the H· produces H_2 gas, whereas the HO· serves as the precursors for O_2 generation.

$$OH^{\cdot} + OH^{\cdot} \rightarrow H_2O + {}^1/_2O_2 \quad \left(\text{Formation of } O_2\right), \quad (4)$$

$$H^{\cdot} + H^{\cdot} \rightarrow H_2 \quad \left(\text{Formation of } H_2\right). \quad (5)$$

The comparison of the time-scale release of H_2 and O_2, as determined by GC analysis, during the exposure of

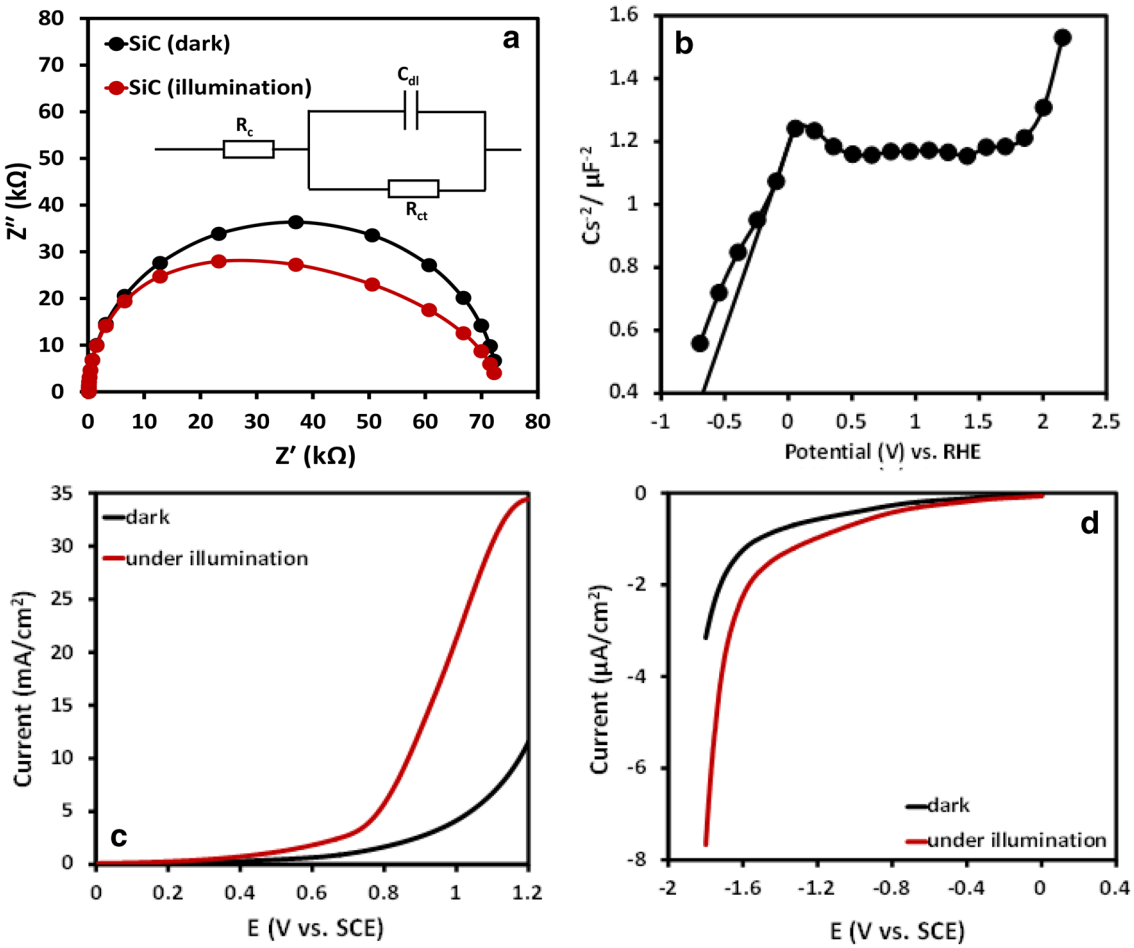

Fig. 7 The comparison of the **a** EIS spectra and **b** Mott–Schottky plot **c** water oxidation and **d** hydrogen evolution of as-synthesized SiC. The graphical evaluation of the flat band (V_{fb}) potential is also elaborated in **b**

as-synthesized SiC to medium pressure mercury pressure lamp operated at 300-W, in the neutral water, is presented in Fig. 8a where a linear increase in the release of H_2 was noticed in the initial 90 min of exposure followed by the loss of linearity and gradual decrease. A maximum yield of 17.5 µmol was evaluated in 150 min of exposure. On the other hand, a consistent increase in the production of O_2 was witnessed with the increasing exposure time. Interestingly, the optimum ratio of 1:2 was not achieved. The simultaneous release of both the gasses authenticated the oxidation of adsorbed water molecules (Eq. 2), reduction of H^+ ions (Eq. 3), inhalation of H• to produce hydrogen (Eq. 4) and coupling of HO· radicals to produce O_2 (Eq. 5) at the surface of the synthesized SiC. Additionally, the aptness of the redox potentials associated with the valence and conduction band edges and the suitability of the adopted procedure for the determination of the flat band potential was also established. The increase in the concentration of H_2 followed by the decrease afterward indicated the decreased formation of H· radicals, the precursors for H_2, with time. On the other hand, although non-linear, however, consistent increase in the concentration of O_2 unveiled the sustained water oxidation in the system. It might be anticipated that the initial linear increase in the concentration of H_2 is primarily due to the absence of oxygen as being pushed out the system by argon purging. On the other hand, the increase in the concentration of O_2 in the solution with the increasing exposure time (Eq. 2), as both having the suitable reduction potentials, initiates the competition between the H^+ ions and the adsorbed O_2 molecules for the conduction band electrons that results in the formation of superoxide anions ($O_2 \cdot^-$) that not only retards the formation of H· radicals but consequently H_2 gas. The interaction of negatively charged superoxide anion radical in the bulk with the H^+ ions, as given in the equations below, further affect the yield of H_2 and enhance the yield of O_2. The pictorial representation of the cumulative process is presented in the Scheme 1 below.

The use of metal ion with suitable redox potential for enhancing the photocatalytic activity is primitive. The metal ions in the solution target the conduction band electrons

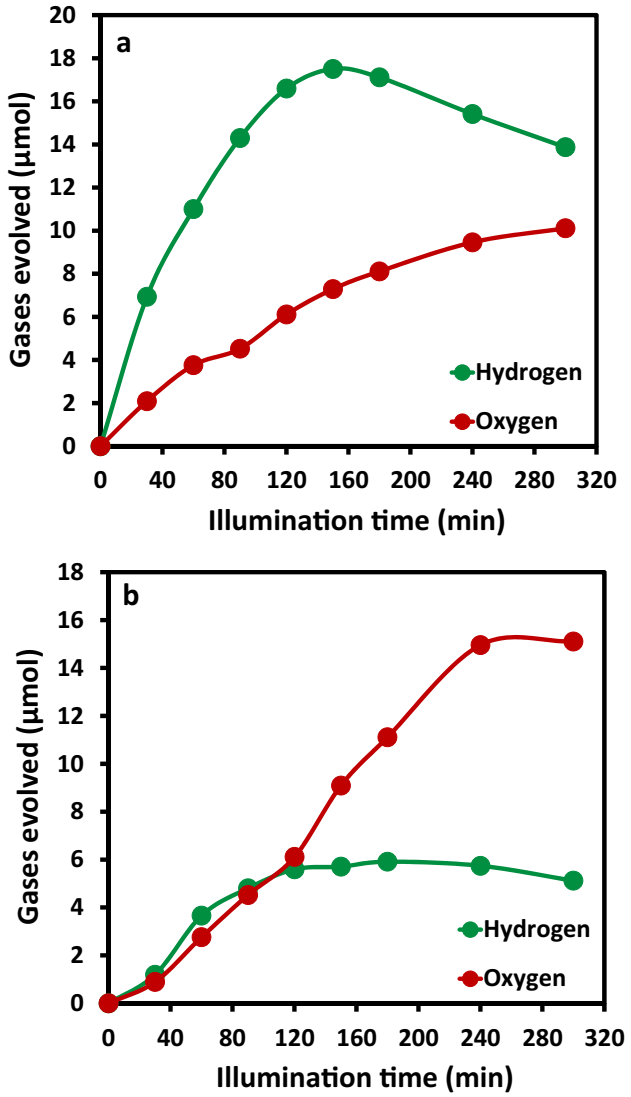

Fig. 8 The comparison of the evolution of H_2 and O_2 gases during the **a** photocatalytic water-splitting process over as-synthesized SiC in the exposure of 300 W medium pressure lamp. **b** The effect of Fe^{3+} ions on the production of gases under identical experimental conditions

among the photon-generated excitons, thus, enhancing the lifetime of the excited states and often termed as "electron-capture agents". In the current study, the effect of the electron-capture abilities of Fe^{3+} ions having the reduction potential of +0.77 V (Fe^{3+}/Fe^{2+}) was investigated on the generation of H_2 and O_2. Due to the non-availability of the conduction band electrons for the H^+ ions produced in situ as a consequence of the water oxidation, a decrease in the yield of H_2, whereas a subsequent increase in the O_2 evolution was anticipated. As presented in Fig. 8b, as a consequence of the electron-capture action of the Fe^{3+}, leading to the formation of Fe^{2+} ions in the system, a substantial decrease in the yield of H_2 was observed. The maximum concentration of ~17.8 µmol of H_2 (in 150 min of exposure) produced in the absence of metal ions was dropped to ~5.7 µmol in the presence of Fe^{3+} ions. Surprisingly, in the initial 90 min of exposure, the yield of O_2 was also considerably lower, whereas a considerable increase in the rate of O_2 production was noticed afterward. The effect is explainable on the basis of the fact that the reduction of Fe^{3+} ions by the conduction band electrons initiates the formation of Fe^{2+} ions with the associated oxidation potential of −0.783 V. Due to the highly suitable oxidation potential, the priority interaction of Fe^{2+} ions with the photogenerated holes results in the reduced oxidation of adsorbed water molecules. The competition between the water molecules and the in situ-generated Fe^{2+} entities severely affect the formation of HO· radicals that serve as precursors for O_2 formation (Eq. 4). The sharp increase in O_2 production after 90 min of exposure indicates the involvement of additional processes that contribute to the formation of O_2. As Fe^{3+}/Fe^{2+} undergo oxidation–reduction under illumination in the aqueous medium, the possible involvement of the photo-Fenton-type reaction (Ruppert et al. 1993) in enhancing the yield of O_2 was anticipated. The above discussion is explainable by Eqs. (6–8) below.

$$Fe^{3+} + e^{-}_{cb} \rightarrow Fe^{2+}, \tag{6}$$

$$Fe^{2+} + h^{+}_{vb} \rightarrow Fe^{3+}, \tag{7}$$

$$Fe^{2+} + H_2O_2 + H^+ \rightarrow Fe^{3+} + OH^{\cdot} + H_2O. \tag{8}$$

Besides electron-capture agent, the lifetime of the excited states might be enhanced by the hole scavengers. Methanol, due to high affinity as compared to water, is well recognized as the h^+ capture agent. The time-scale profile of the released gasses during the water splitting in the presence of 1% (by volume) of methanol is presented in Fig. 9a. A substantial increase in the production of H_2 as compared to that of pure water was witnessed. Compared to ~17.5 µmol in 150 min of exposure, ~90 µmol of H_2 were evolved in the same period. A considerable decrease in the release of O_2 was also witnessed. Besides H_2 and O_2, the formation of CO and CH_4 was also observed. The observation demonstrated that the holes (h^+) prioritize the oxidation of the added CH_3OH to produce H^+ ions as compared to the adsorbed water. The low formation of O_2 offer less competition to the methanol-generated H^+ ions for the capture of conduction band electrons thus escalating the formation of H_2 gas in the system. Additionally, the hydrogen-rich CH_3OH produces a higher number of H^+ ions as compared to water molecules. The high yield of H_2 and the formation of CO in the acceptable concentration, in the system, suggest multiple oxidations of the secondary products of initial oxidation of CH_3OH till the complete stripping of the H^+ ions and the formation of CO. The plausible mechanism of methanol interaction with the h^+ (holes) leading to the enhanced formation of H^+

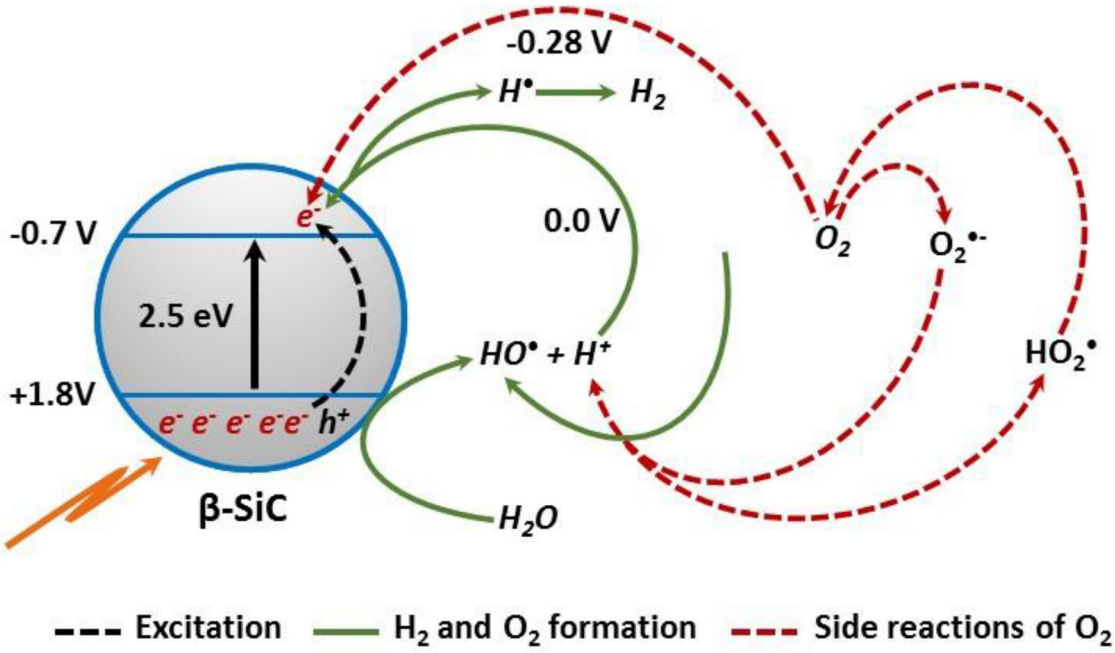

Scheme 1 The plausible mechanism of the photocatalytic generation of H_2 and O_2 as a result of water splitting

ions and CO in the system, similar to that proposed for the electro-oxidation of methanol, is suggested as below.

$$CH_3OH + h^+_{vb} \rightarrow CH_3O^+H \rightarrow CH_2O + H^+ + H^{\cdot}, \quad (9)$$

$$CH_2O + h^+_{vb} \rightarrow CH_2O^+ \rightarrow CO + H^{\cdot} + H^+. \quad (10)$$

In the presence of H· in the system, the formation of CH_4 gas is equally probable due to inevitable interaction with the methanol molecules.

The process was further investigated in the presence of both 1% methanol (hole scavenger) and 50 ppm of Fe^{3+} ions (electron scavenger) in the aqueous medium over as-synthesized SiC. The profiles of the evolved gases are presented in Fig. 9b, where the formation of H_2, O_2, CO and CH_4 in the varying concentrations is observable. Interestingly, the extremely low concentration of CO_2 was also observed. The presence of simultaneous presence of both methanol and Fe^{3+} ions in the solutions resulted in a complex picture. Although considerably higher than that measured for pure H_2O and with 50 ppm Fe^{3+} ions, however, the yield of H_2 was significantly lower than that observed with 1% methanol solution. Considering Eqs. (9) and (10), the oxidation of methanol and secondary offshoot (formaldehyde) leads to the generation of radical (H·) and ionic (H^+) entities. It seems quite obvious that the observed H_2 is merely due to the coupling of the radical species generated due to the oxidation of methanol, whereas the H^+ ions fail to be transformed to H· due to the presence of Fe^{3+} ions. The enhanced formation of CO clearly indicates that due to the electron capture action of Fe^{3+} ions, the life expectancy of the excited states is prolonged that ensure the ample availability of h^+ for the oxidation of methanol and formaldehyde.

The reusability of the synthesized catalyst was examined by exposing the same catalyst after the interval of 48 h and monitored the release of H_2 gas. The catalysts showed the sustained activity in the successive cycles.

Conclusions

The study proposed the n-type β-SiC as the potential candidate for the photocatalytic water splitting. A sustained generation of H_2 was observed in the absence of appreciable O_2 in the system that decreased with the in situ formation of O_2. The use of oxygen-scavenging entities might be helpful in this regard. The electron scavenging role of Fe^{3+} ions and their established character in the photo-fenton-type reactions enhanced the formation of O_2 by suppressing the generation of H_2. In competition with H_2O, the study also established the h^+ scavenging ability of methanol as the potent source of H^+ ions. The multiple oxidations of the offshoots and the generation of a variety of entities result in the formation of CO and CH_4 in the system.

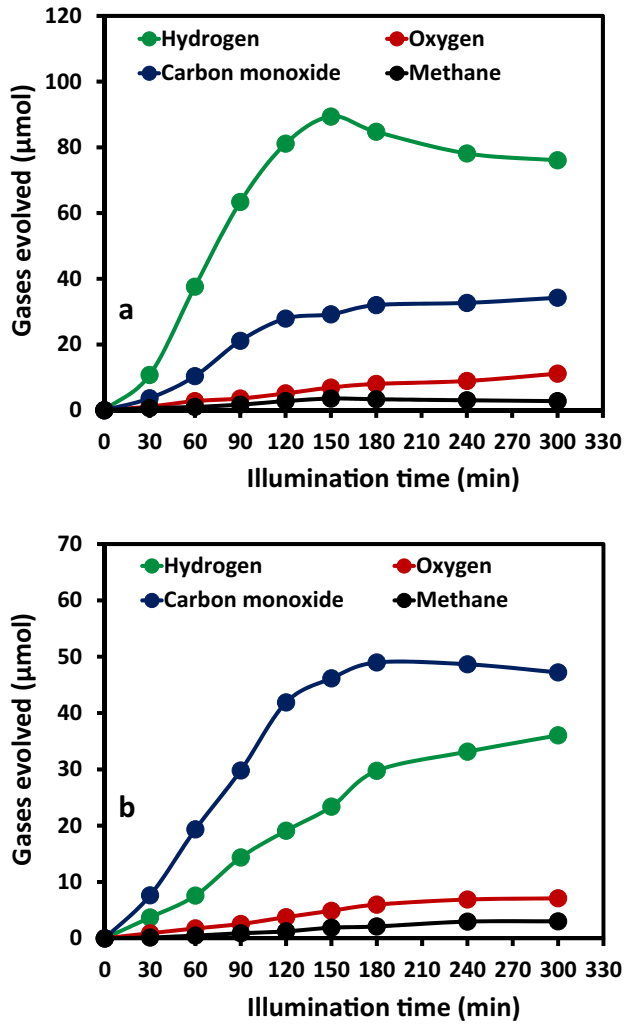

Fig. 9 **a** The comparison of the evolved gases from **a** 1% methanol solution **b** 1% methanol solution + 50 ppm of Fe^{3+} ions over as-synthesized SiC in the exposure of 300 W medium pressure lamp

Acknowledgements A. Hameed and M. Aslam are thankful to Center of Excellence in Environmental Studies (CEES), King Abdulaziz University, Kingdom of Saudi Arabia for technical support.

Compliance with ethical standards

Conflict of interest The authors declare no conflict of interest.

References

Ahmad H, Kamarudin SK, Minggu LJ, Kassim M (2015) Hydrogen from photo-catalytic water splitting process: a review. Renew Sustain Energy Rev 43:599–610

Balat H, Kırtay E (2010) Hydrogen from biomass-present scenario and future prospects. Int J Hydrog Energy 35:7416–7426

Çelik D, Yıldız M (2017) Investigation of hydrogen production methods in accordance with green chemistry principles. Int J Hydrog Energy 42:23395–23401

Chang F, Zheng J, Wang X, Xu Q, Deng B, Hu X, Liu X (2018) Heterojuncted non-metal binary composites silicon carbide/g-C_3N_4 with enhanced photocatalytic performance. Mater Sci Semicond Process 75:183–192

Chen X, Shen S, Guo L, Mao SS (2010) Semiconductor-based photocatalytic hydrogen generation. Chem Rev 110:6503–6570

Chen Z, Bing F, Liu Q, Zhang Z, Fang X (2015) Novel Z-scheme visible-light-driven Ag_3PO_4/Ag/SiC photocatalysts with enhanced photocatalytic activity. J Mater Chem A 3:4652–4658

Chen S, Takata T, Domen K (2017) Particulate photocatalysts for overall water splitting. Nat Rev Mater 2:17050

Dang H, Li B, Li C, Zang Y, Xu P, Zhao X, Fan H, Qiu Y (2018) One-dimensional Au/SiC heterojunction nanocomposites with enhanced photocatalytic and photoelectrochemical performances: kinetics and mechanism insights. Electrochim Acta 267:24–33

Fan J, Chu PK (2014) Silicon carbide nanostructures: fabrication, structure, and properties. Springer International Publishing, Switzerland

Frei H (2017) Photocatalytic fuel production. Curr Opin Electrochem 2:128–135

Freitas JA Jr (1995) Photoluminescence spectra of SiC poly types, in properties of silicon carbide. In: Harris GL (ed) EMIS Data Rev Series No. 13, pp 29–41

Freitas JA Jr, Moore WJ (1998) Optical studies of undoped and doped wide bandgap carbide and nitride semiconductors. Braz J Phys 28:12–18

Fu QG, Li HJ, Shi XH, Li KZ, Sun GD (2005) Silicon carbide coating to protect carbon/carbon composites against oxidation. Scr Mater 52:923–927

Fujishima A, Honda K (1971) Electrochemical evidence for the mechanism of the primary stage of photosynthesis. Bull Chem Soc Jpn 44:1148–1150

Hao JY, Wang YY, Tong XL, Jin GQ, Guo XY (2013) SiC nanomaterials with different morphologies for photocatalytic hydrogen production under visible light irradiation. Catal Today 212:220–224

Hatakeyama F, Kanzaki S (1990) Synthesis of monodispersed spherical β-silicon carbide powder by a sol–gel process. J Am Ceram Soc 73:2107–2110

Hisatomi T, Domen K (2017) Progress in the demonstration and understanding of water splitting using particulate photocatalysts. Curr Opin Electrochem 2:148–154

Huang Q, Chen X, Liu J, Wang W, Wang G, Wang W, Yang R, Liu Y, Guo L (2010) Epitaxial graphene on 4H-SiC by pulsed electron irradiation. Chem Commun 46:4917–4919

Ishikawa T, Kohtoku Y, Kumagawa K, Yamamura T, Nagasawa T (1998) High-strength alkali-resistant sintered SiC fibre stable to 2200 °C. Nature 391:773–775

Iwanowski RJ, Fronc K, Paszkowicz W, Heinonen M (1999) XPS and XRD study of crystalline 3C-SiC grown by sublimation method. J Alloys Compds 286:143–147

Jiang M, Liu Z, Ding L, Chen J (2017) Facile fabrication and efficient photoelectrochemical water-splitting activity of electrodeposited nickel/SiC nanowires composite electrode. Catal Commun 96:46–49

Kothari R, Buddhi D, Sawhney RL (2008) Comparison of environmental and economic aspects of various hydrogen production methods. Renew Sustain Energy Rev 12:553–563

Kudo A, Miseki Y (2009) Heterogeneous photocatalyst materials for water splitting. Chem Soc Rev 38:253–278

Lauermann I, Memming R, Meissner D (1997) Electrochemical properties of silicon carbide. J Electrochem Soc 144:73–80

Lee CP, Luna LE, DelaCruz S, Ortaboy S, Rossi F, Salviati G, Carraro C, Maboudian R (2018) Hierarchical cobalt oxide-functionalized

silicon carbide nanowire array for efficient and robust oxygen evolution electro-catalysis. Mater Today Energy 7:37–43
Li J, Tian J, Dong L (2000) Synthesis of SiC precursors by a two-step sol–gel process and their conversion to SiC powders. J Eur Ceram Soc 20:1853–1857
Lin S, Chen Z, Li L, Ba Y, Liu S, Yang M (2012) Investigation of micropipes in 6H-SiC by Raman scattering. Phys B 407:670–673
Liu H, She G, Mu L, Shi W (2012) Porous SiC nanowire arrays as stable photocatalyst for water splitting under UV irradiation. Mater Res Bull 47:917–920
Madar R (2004) Materials science: silicon carbide in contention. Nature 430:974–975
Maeda K, Domen K (2010) Photocatalytic water splitting: recent progress and future challenges. J Phys Chem Lett 1:2655–2661
Mikolaj S, Pawel W (2001) Effect of the bonding ceramic material on the size of pores in porous ceramic materials. Colloids Surf A Physicochem Eng Asp 179:201–208
Moon SC, Mametsuka H, Tabata S, Suzuki E (2000) Photocatalytic production of hydrogen from water using TiO_2 and B/TiO_2. Catal Today 58:125–132
Muradova NZ, Veziroğlub TN (2008) "Green" path from fossil-based to hydrogen economy: an overview of carbon-neutral technologies. Int J Hydrog Energy 33:6804–6839
Najafi A, Golestani Fard F, Rezaie HR, Ehsani N (2012) Synthesis and characterization of SiC nano powder with low residual carbon processed by sol–gel method. Powder Technol 219:202–210
Nakamura D, Gunjishima I, Yamaguchi S, Ito T, Okamoto A, Kondo H, Onda S, Takatori K (2004) Ultrahigh-quality silicon carbide single crystals. Nature 430:1009–1012
Ni M, Leung MKH, Leung DYC, Sumathy K (2007) A review and recent developments in photocatalytic water-splitting using TiO_2 for hydrogen production. Renew Sustain Energy Rev 11:401–425
Peng Y, Guo Z, Yang J, Wang D, Yuan W (2014) Enhanced photocatalytic H_2 evolution over micro-SiC by coupling with CdS under visible light irradiation. J Mater Chem A 2:6296–6300
Persson C, Lindefelt U (1997) Relativistic band structure calculation of cubic and hexagonal SiC polytypes. J Appl Phys 82:5496–5508
Pierre M (2002) Silicon carbide and silicon carbide-based structures: the physics of epitaxy. Surf Sci Rep 48:1–51
Qamar MT, Aslam M, Rehan ZA, Soomro MT, Ahmad I, Ishaq M, Ismail IMI, Fornasiero P, Hameed A (2017) MoO_3 altered ZnO: a suitable choice for the photocatalytic removal of chloro-acetic acids in natural sunlight exposure. Chem Eng J 330:322–336
Qi X, Zhai G, Liang J, Ma S, Liu X, Xu B (2014) Preparation and characterization of SiC@CNT coaxial nanocables using CNTs as a template. CrystEngComm 16:9697–9703
Raman V, Bahl OP, Dhawan U (1995) Synthesis of silicon carbide through the sol–gel process from different precursors. J Mater Sci 30:2686–2693
Ravi BG, Omotoye OA, Srivatsan TS, Petrorali M, Sudarshan TS (2000) The microstructure and hardness of silicon carbide synthesized by plasma pressure compaction. J Alloys Compd 299:292–296
Ruppert G, Bauer R, Heisler G (1993) The photo-Fenton reaction—an effective photochemical wastewater treatment process. J Photochem Photobiol A Chem 73:75–78
Sachsenhauser M, Sharp ID, Stutzmann M, Garrido JA (2016) Surface state mediated electron transfer across the *n*-type SiC/electrolyte interface. J Phys Chem C 120:6524–6533
Saraswat SK, Rodene DD, Gupta RB (2018) Recent advancements in semiconductor materials for photoelectrochemical water splitting for hydrogen production using visible light. Renew Sustain Energ Rev 89:228–248
Shankar S (2017) Renewable and nonrenewable energy resources: bioenergy and biofuels. In: Singh RL (ed) Principles and applications of environmental biotechnology for a sustainable future. Springer Singapore, Singapore, pp 293–314
Shcherban ND (2017) Review on synthesis, structure, physical and chemical properties and functional characteristics of porous silicon carbide. J Ind Eng Chem 50:15–28
Shi L, Zhao H, Yan Y, Li Z, Tang C (2006) Synthesis and characterization of submicron silicon carbide powders with silicon and phenolic resin. Powder Technol 169:71–76
van Dorp DH, Hijnen N, Di Vece M, Kelly JJ (2009) SiC: a photocathode for water splitting and hydrogen storage. Angew Chem Int Ed 48:6085–6088
Walter MG, Warren EL, McKone JR, Boettcher SW, Mi Q, Santori EA, Lewis NS (2010) Solar water splitting cells. Chem Rev 110:6446–6473
Wang Y, Guo X, Dong L, Jin G, Wang Y, Guo XY (2013) Enhanced photocatalytic performance of chemically bonded SiC–graphene composites for visible-light-driven overall water splitting. Int J Hydrog Energy 38:12733–12738
Wang M, Chen J, Liao X, Liu Z, Zhang J, Gao L, Li Y (2014a) Highly efficient photocatalytic hydrogen production of platinum nanoparticle-decorated SiC nanowires under simulated sunlight irradiation. Int J Hydrog Energy 39:14581–14587
Wang M, Chen J, Liao X, Liu Z, Zhang J, Gao L, Li Y (2014b) Highly efficient photocatalytic hydrogen production of platinum nanoparticle-decorated SiC nanowires under simulated sunlight irradiation. Int J Hydrog Energy 39:14581–14587
Wang B, Zhang J, Huang F (2017a) Enhanced visible light photocatalytic H_2 evolution of metal-free g-C_3N_4/SiC heterostructured photocatalysts. Appl Surf Sci 391:449–456
Wang D, Wang W, Wang Q, Guo Z, Yuan W (2017b) Spatial separation of Pt and IrO_2 cocatalysts on SiC surface for enhanced photocatalysis. Mater Lett 201:114–117
Wanga YY, Kusumotob K, Lia CJ (2012) XPS analysis of SiC films prepared by radio frequency plasma sputtering. Phys Proc 32:95–102
Wenzien B, Käckell P, Bechstedt F, Cappellini G (1995) Quasiparticle band structure of silicon carbide polytypes. Phys Rev B 52:10897–10905
Xie Y, Yang J, Chen Y, Liu X, Zhao H, Yao Y, Cao H (2018) Promising application of SiC without co-catalyst in photocatalysis and ozone integrated process for aqueous organics degradation. Catal Today. https://doi.org/10.1016/j.cattod.2018.01.013
Xue K, Niu L, Shi H, Liu J (2008) Structural relaxation of amorphous silicon carbide thin films in thermal annealing. Thin Solid Films 516:3855–3861
Yasuda T, Kato M, Ichimura M, Hatayama T (2012) SiC photoelectrodes for a self-driven water-splitting cell. Appl Phys Lett 101:053902
Yoshida K, Budiyanto Imai M, Yano T (1998) Processing and microstructure of silicon carbide fiber-reinforced silicon carbide composite by hot-pressing. J Nucl Mater 258–263:1960–1965
Zhang Y, Xia T, Wallenmeyer P, Harris CX, Peterson AA, Corsiglia GA, Murowchick J, Chen X (2014) Photocatalytic hydrogen generation from pure water using silicon carbide nanoparticles. Energy Technol 2:183–187
Zhu XW, Jiang DL, Tan SH (2001) Improvement in the strength of reticulated porous ceramics by vacuum degassing. Mater Lett 51:363–367
Zhu F, Hu J, Matulionis I, Deutsch T, Gaillard N, Kunrath A, Miller E, Madan A (2009) Amorphous silicon carbide photoelectrode for hydrogen production directly from water using sunlight. Philos Mag 89:2723–2739